9. Markers for dominant and recessive hearing loss loci are listed on the Hereditary Hearing Loss Homepage (G. Van Camp and R. J. H. Smith, January 1998; Web site, http://dnalab-www.uia.ac.be/dnalab/hhh). Blood (20 cm^3) was collected from each individual; DNA was made from 10 cm^3 of each sample [S. A. Miller, D. D. Dykes, H. F. Polesky, *Nucleic Acids Res.* **16**, 1215 (1988)], and the remaining 10 cm^3 was used for establishing lymphoblastoid cell lines [H. Neitzel, *Hum. Genet.* **73**, 320 (1986)].
10. PCR amplification and genotyping of polymorphic markers were carried out as described (*4*).
11. Linkage was evaluated using LINKAGE v5.1 (G. M. Lathrop, J. M. Lalouel, C. Julier, J. Ott, *Proc. Natl. Acad. Sci. U.S.A.* **81**, 3443 (1984)] and FASTLINK v3.0P [R. W. Cottingham Jr., R. M. Idury, A. A. Schaffer, *Am. J. Hum. Genet.* **53**, 252 (1993)].
12. K. P. Steel and S. D. M. Brown, *Trends Genet.* **10**, 428 (1994).
13. F. Gibson *et al.*, *Nature* **374**, 62 (1995).
14. Y.-R. Xia *et al.*, *Genomics.* **18**, 126 (1993); T. Theil, U. Zechner, C. Klett, S. Adolph, T. Moroy, *Cytogenet. Cell Genet.* **66**, 267 (1994); N. G. Copeland *et al.*, *Science* **262**, 57 (1993); Mouse Genome Database at the Jackson Laboratory (Web site, www.informatics.jax.org).
15. L. Erkman *et al.*, *Nature* **381**, 603 (1996).
16. M. Xiang *et al.*, *Proc. Natl. Acad. Sci. U.S.A.* **94**, 9445 (1997).
17. Primers were designed to amplify the human *POU4F3* gene by means of sequence information for the two coding exons available from GenBank (accession numbers U10060 and U10061) and sequence we obtained on the intron separating the two exons (GenBank accession number AF043452). Sequence of the fragment generated by PCR using the primer pair 629F (5′-CGGCTCTGGCTAATCTCAAG-3′) and 939R (5′-AAGGTCCAGTTTCTCAGCGA-3′) revealed a deletion in affected individuals (Fig. 2, A and B). The deletion was confirmed in all affected Family H members both by screening for single-strand conformation polymorphisms (SSCPs) and by separation of alleles on 3% MetaPhor gels (FMC), using primers spanning the deletion of *POU4F3* (Fig. 2C). Variant bands obtained from SSCP, using PCR primers to amplify the *POU4F3* region that includes the H family deletion, were gel-purified, reamplified, and sequenced as described (*4*).
18. Primers 629F and 939R surrounding the deletion in affected Family H members were used to amplify genomic DNA. The product was labeled by incorporation of [α-^{32}P]deoxyguanosine triphosphate during PCR. Each sample was loaded onto a 6% polyacrylamide denaturing gel and electrophoresed at 70 W for 4.5 hours to resolve the 310-bp (wild-type) and 302-bp (Family H mutant allele) fragments. Gels were dried and exposed to x-ray film.
19. Northern blots containing 2 μg of polyadenylated RNA from 16 different human tissues were hybridized with a portion of the human *POU4F3* cDNA (Multiple Tissue Northern I and II, Clontech) according to the manufacturer's protocol. The probe was a PCR-generated fragment of *POU4F3* exon 2 (nucleotides 629 to 939).
20. Total RNA from human fetal cochlea, brain, and kidney was extracted using the guanidine isothiocyanate method [J. M. Chirgwin, A. E. Przybyla, R. J. MacDonald, W. Rutter, *Biochemistry* **18**, 5294 (1979)]. Total RNA (3 μg) was reverse-transcribed with the SuperScript II kit (Gibco-BRL). Parallel PCR reactions with reverse transcriptase (+RT) and without reverse transcriptase (–RT) were performed to evaluate DNA contamination in RNA samples. Reverse transcriptase (+/– RT) reaction was used as a template for PCR. The following PCR primers spanning the 314-bp intron were used: 48F (5′-TGCAAGAACCCAAATTCTCC-3′) to 804R (5′-GAGCTCTGGCTTGCTGTTCT-3′). A 756-bp product was observed in cochlear RNA, corresponding to the cDNA size. Genomic DNA contamination was present in all samples, as shown by the 1070-bp band observed in all lanes (Fig. 2E). PCR reagents including Taq polymerase (Perkin-Elmer) were used according to the manufacturer's instructions.
21. M. Xiang *et al.*, *J. Neurosci.* **15**, 4762 (1995); M. R. Gerrero *et al.*, *Proc. Natl. Acad. Sci. U.S.A.* **90**, 10841 (1993); N. N. Ninkina, G. E. M. Stevens, J. N. Wood, W. D. Richardson, *Nucleic Acids Res.* **21**, 3175 (1993).
22. M. Wegner, D. W. Drolet, M. G. Rosenfeld, *Curr. Opin. Cell Biol.* **5**, 488 (1993).
23. C. A. Gruber, J. M. Rhee, A. Gleiberman, E. E. Turner, *Mol. Cell. Biol.* **17**, 2391 (1997).
24. H. A. Ingraham *et al.*, *Cell* **61**, 1021 (1990); M. C. Botfield, A. Jancso, M. A. Weiss, *Biochemistry* **31**, 5841 (1992); C. P. Verrijzer *et al.*, *EMBO J.* **11**, 4993 (1992).
25. H. Schuknecht, *Pathology of the Ear* (Harvard Univ. Press, Cambridge, MA, 1974).
26. L. E. Maquat, *Am J. Hum. Genet.* **59**, 279 (1996).
27. J. D. Klemm, M. A. Rould, R. Aurora, W. Herr, C. O. Pabo, *Cell* **77**, 21 (1994).
28. Alteration of a single residue in the POU homeodomain of Pou4f2 changes this transcription factor from a repressor to an activator of the SNAP-25 promoter; Pou4f3 shares this site with Pou4f2 [P. J. Morris, S. J. Dawson, M. C. Wilson, D. S. Latchman, *Neuroreport* **8**, 2041 (1997)].
29. T. Theil, B. Rodel, F. Spiegelhalter, T. Moroy, *J. Biol. Chem.* **270**, 30958 (1995).
30. A. Ryan, L. Erkman, E. Keithley, personal communication.
31. We thank all Family H members for their cooperation and enthusiasm for this study. We thank T. Sobe and S. Haika for assistance; B. Ploplis, M. Idelson, I. Bejerano-Achache, and M. Mastroianni for technical support; B. Bonne-Tamir, A. Adato, and C. Froehlich for critical advice; I. Ashkenazi and Y. Shiloh for generous support; and G. Van Camp for collecting blood from family members living in Belgium. Supported in part by Tel Aviv University (K.B.A.), NIDCD grant R01 DC01076 (M.-C.K. and E.D.L.), and Intramural Research Project grant Z01 DC 00039 (T.B.F. and R.M.).

5 January 1998; accepted 29 January 1998

FADD: Essential for Embryo Development and Signaling from Some, But Not All, Inducers of Apoptosis

Wen-Chen Yeh, José Luis de la Pompa, Mila E. McCurrach, Hong-Bing Shu, Andrew J. Elia, Arda Shahinian, Michelle Ng, Andrew Wakeham, Wilson Khoo, Kyran Mitchell, Wafik S. El-Deiry, Scott W. Lowe, David V. Goeddel, Tak W. Mak*

FADD (also known as Mort-1) is a signal transducer downstream of cell death receptor CD95 (also called Fas). CD95, tumor necrosis factor receptor type 1 (TNFR-1), and death receptor 3 (DR3) did not induce apoptosis in FADD-deficient embryonic fibroblasts, whereas DR4, oncogenes *E1A* and c-*myc*, and chemotherapeutic agent adriamycin did. Mice with a deletion in the FADD gene did not survive beyond day 11.5 of embryogenesis; these mice showed signs of cardiac failure and abdominal hemorrhage. Chimeric embryos showing a high contribution of *FADD* null mutant cells to the heart reproduce the phenotype of FADD-deficient mutants. Thus, not only death receptors, but also receptors that couple to developmental programs, may use FADD for signaling.

CD95 (the Fas antigen) is a death domain–containing receptor of the TNFR family that signals apoptosis to eliminate unwanted, autoreactive lymphocytes (*1*). Activation of CD95 by either CD95 ligand (CD95L or FasL) or treatment with an agonistic antibody results in receptor aggregation and the rapid recruitment of FADD (Fas-associated death domain protein), a 26-kD cytoplasmic protein with a death domain (*2*). The interaction of FADD and Fas through their COOH-terminal death domains unmasks the NH_2-terminal death effector domain (DED) of FADD, allowing it to recruit caspase-8 to the Fas signaling complex (*3*) and thereby activating a cysteine protease cascade leading to cell death.

FADD and its downstream caspase cascade may also participate in signaling by other members of the TNFR family. TRADD (TNFR-1 associated death domain protein), an adapter protein that binds directly to the death domain of TNFR-1, can transduce signals for apoptosis (*4*). In overexpression systems, FADD is recruited by TRADD to TNFR-1 and DR3 (also called Wsl-1) signaling complexes, and FADD mutants lacking the DED are dominant-negative inhibitors of TNFR-1– and DR3-induced cell death (*5*, *6*).

Outside of cell death signaling and the

W.-C. Yeh, J. L. de la Pompa, A. J. Elia, A. Shahinian, M. Ng, A. Wakeham, W. Khoo, T. W. Mak, Amgen Institute, Departments of Medical Biophysics and Immunology, University of Toronto, and Ontario Cancer Institute, 610 University Avenue, Toronto, Ontario M5G 2C1, Canada.
M. E. McCurrach and S. W. Lowe, Cold Spring Harbor Laboratories, 1 Bungtown Road, Cold Spring Harbor, NY 11724, USA.
H.-B. Shu and D. V. Goeddel, Tularik, 2 Corporate Drive, South San Francisco, CA 94080, USA.
K. Mitchell and W. S. El-Deiry, Howard Hughes Medical Institute, University of Pennsylvania School of Medicine CRB 437A, Philadelphia, PA 19104, USA.

*To whom correspondence should be addressed. E-mail: t.mak@oci.utoronto.ca

immune system, the physiological roles of FADD remain to be characterized. We have now inactivated the *FADD* gene in mice by gene targeting in embryonic stem (ES) cells (Fig. 1, A and B) (*7*). Out of the first 57 live pups genotyped from heterozygous *FADD* matings, no homozygous mutants were observed. Therefore, timed breedings followed by genotyping were done. Up to 9.5 days of gestation (E9.5), viable homozygous *FADD* mutants were present in the expected Mendelian ratio (25.2%). Thereafter, viable *FADD* mutant embryos were obtained at a decreased ratio from E10.5 (18.8%) to E11.5 (4.1%), until all were dead by E12.5. At E11.5, *FADD* mutant embryos were underdeveloped and showed signs of abdominal hemorrhage (Fig. 1C). *FADD* mRNA was expressed in wild-type (WT) ES cells and throughout development (Fig. 1D). Protein expression, however, was decreased in the day E9.5 heterozygous fibroblasts and completely absent in homozygous mutants (Fig. 1E), indicating that the *FADD* mutation was null.

The spatial distribution of *FADD* between days E9.5 and E12.5 of development was analyzed by in situ hybridization (*8*). At E10, *FADD* mRNA was expressed widely, consistent with its involvement in developmental processes in the embryo (Fig. 2A). Mutant embryos did not show any *FADD* signal (Fig. 2B), consistent with the protein immunoblot results. At E11.5, *FADD* expression was concentrated in the brain (Fig. 2, C and D), myocardium (Fig. 2, C and E), liver (Fig. 2, C and F), and the developing vertebrae (Fig. 2, C and G). Histological analyses of these tissues between E9.5 and E11.5 revealed that at E10.5 (Fig. 3, A and C), in ~80% of the *FADD* mutant embryos, the ventricular myocardium was thinner than in their WT littermates (Fig. 3, B and D). In addition, the inner trabeculation was poorly developed (Fig. 3D) (*9*). In contrast, the endocardial cushions appeared normal (Fig. 3D). Chorioallantoic fusion occurred normally in *FADD* mutant embryos (*10*); thus, their developmental delay was not associated with abnormal placental development.

Because ~50% of the mutant embryos surviving at E11.5 were hemorrhagic, we examined the development of the vascular endothelium by breeding into the *FADD* mutant background a mutation for the receptor tyrosine kinase Flk1, an early endothelial marker (*11*). In generating the targeted mutation of the *flk1* gene, the *lacZ* gene was knocked-in, allowing the assessment of *flk1* expression in $FADD^{-/-}$ and WT embryos by β-galactosidase (β-Gal) staining (*12*). The vascular endothelium was clearly delineated in both the $FADD^{+/+}$;$flk1^{-/+}$ and $FADD^{-/-}$;$flk1^{-/+}$ embryos (Fig. 3, G and H). Therefore, the hemorrhage observed in mutant embryos was unlikely to be due to the abnormal development of blood vessels.

Because ~80% of *FADD* mutant embryos exhibited a delayed and underdeveloped phenotype, we investigated whether there

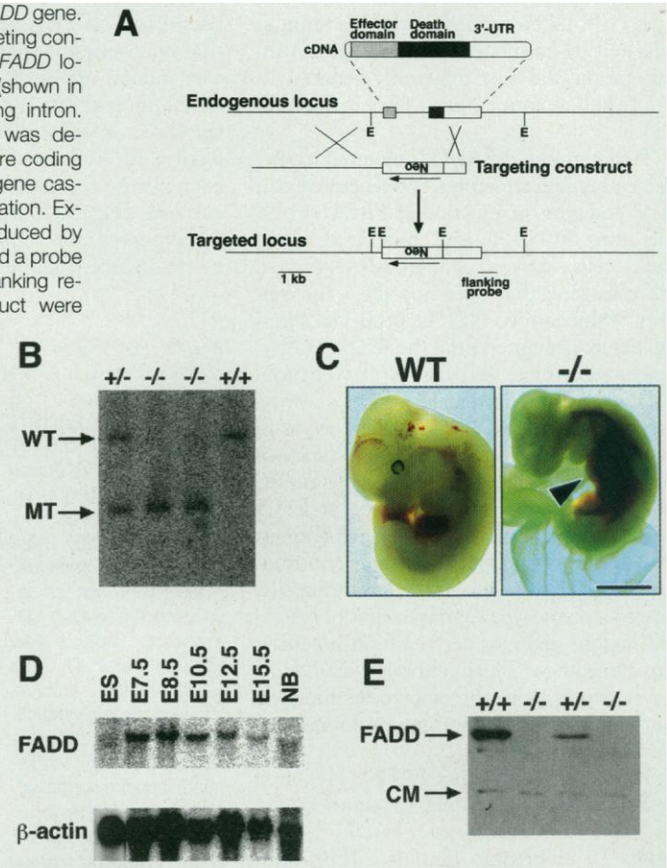

Fig. 1. Targeting of the *FADD* gene. (**A**) Design of a *FADD* targeting construct. The endogenous *FADD* locus contains two exons (shown in boxes) and an intervening intron. The targeting construct was designed to replace the entire coding region with a *PGK-Neo* gene cassette in the reverse orientation. Extra Eco RI sites (E) introduced by the *PGK-Neo* cassette and a probe (flanking probe) in the flanking region outside the construct were used for the diagnosis of homologous recombination. (**B**) Southern blot analysis of DNA derived from WT, $FADD^{+/-}$, and $FADD^{-/-}$ animals. DNA was digested with Eco RI, fractionated on a 0.8% agarose gel, blotted to a nylon membrane (Hybond N, Amersham), and probed with the radiolabeled flanking probe (A). MT, mutant. (**C**) E11.5 WT (left) and *FADD* mutant (right) embryos. The reduced size of the mutant embryo is apparent. The arrowhead points to the hemorrhagic abdominal region. Bar, 500 μm. (**D**) Northern blot analysis of *FADD* gene expression during embryo development. Total RNA (10 μg) from each of the successive stages of embryo development was fractionated on a 1% denatured agarose gel, blotted to a nylon membrane, hybridized with a FADD full-length cDNA probe, and then reprobed with the β-actin cDNA. ES, embryonic stem cells; E7.5, embryonic day 7.5 after fertilization; NB, newborn. (**E**) Protein immunoblot analysis of FADD protein expression. Equal amounts of total protein lysates from WT, $FADD^{+/-}$, and $FADD^{-/-}$ mice were fractionated on a 15% denatured polyacrylamide gel, and the protein immunoblot was probed with a FADD-specific polyclonal antibody. CM, cross-reacting material.

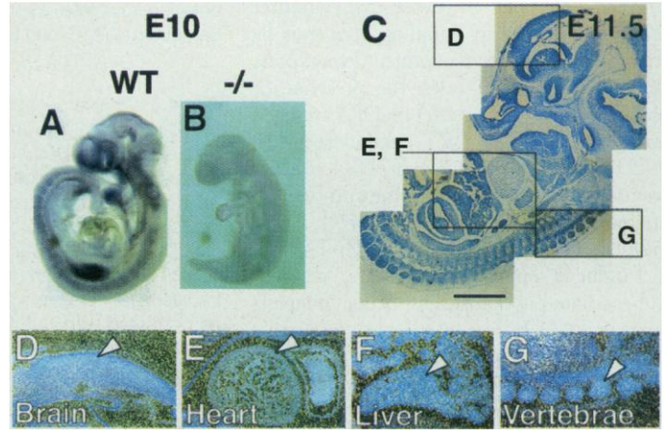

Fig. 2. Widespread *FADD* expression during embryonic development. (**A**) Whole mount in situ hybridization in a WT E10 embryo. *FADD* expression (purple) is detected in all tissues, particularly in the brain, developing somites, and facial mesenchyme. No signal is found in *FADD* mutant embryos (**B**). (**C**) Radioactive in situ hybridization. General bright-field view of an E11.5 WT embryo. (D) to (G) correspond to the insets shown in higher magnification as dark-field views. (**D** to **G**) *FADD* expression in the brain (D, arrowhead), myocardium (E, arrowhead), liver (F, arrowhead), and developing vertebrae (G, arrowhead). The bright cells in the atrial cavity in (E) are unlabeled, refracting red blood cells. Bar, 200 μm (A and B), 1.3 mm (C), and 250 μm (D to G).

was an excess of apoptosis or reduced cellular proliferation. Apoptosis as measured by terminal deoxynucleotidyl transferase–mediated dUTP nick-end labeling (TUNEL) staining was not increased in *FADD* null mutant embryos (*10*). Likewise, cellular proliferation as indicated by bromodeoxyuridine (BrdU) incorporation was not drastically reduced in *FADD* null mutant embryos (Fig. 3, E and F) (*13*).

To determine if *FADD* is required in specific embryonic structures, we generated chimeric embryos by injection of $FADD^{-/-}$ ES cells into *ROSA26 lacZ* blastocysts (*14*). These cells carry a ubiquitously expressed *lacZ* transgene that does not affect the viability of the embryo (*12*). Upon β-Gal staining, tissues generated from the recipient blastocysts stain blue, and tissues derived from $FADD^{-/-}$ ES cells remain white, allowing discrimination between the contributions of mutant and WT embryonic cells. Embryos with a low contribution from the mutant ES cells showed a normal phenotype at E11.5 (*10*). Conversely, embryos with high chimerism (mostly white), all with high contributions of $FADD^{-/-}$ cells in the heart (Fig. 3I), showed a phenotype similar to that of *FADD* null mutant embryos derived from heterozygous breedings. Thus, although *FADD* is widely expressed in the embryo, its function may be particularly important for normal cardiac development.

To determine whether FADD is required for Fas-mediated apoptosis, we transfected a Fas expression vector into $FADD^{-/-}$ and $FADD^{+/+}$ embryonic fibroblast (EF) cells. After 15 hours, essentially all of the Fas-transfected FADD-deficient EF cells were alive, whereas only half of the Fas-transfected WT cells survived. Treatment of the transfected cells with an agonistic antibody to Fas further enhanced killing of the $FADD^{+/+}$ EF cells (Fig. 4A). Expression vectors for TNFR-1, DR3 (6), and DR4 (*15*) were transfected into the EF lines to determine whether FADD is involved in signaling apoptosis by other death domain receptors. Overexpression of either TNFR-1 (in the presence or absence of TNF treatment) or DR3 induced more apoptosis in WT cells than in $FADD^{-/-}$ cell lines. However, DR4 overexpression killed FADD-expressing and FADD-deficient cells equally well (Fig. 4A). Thus, FADD is required for Fas-, TNFR-1–, and DR3-induced apoptosis pathways, whereas DR4-mediated apoptosis can occur independently of FADD.

Furthermore, consistent with other reports (3, 5, 6), overexpression of TRADD did not cause apoptosis in FADD-deficient EF cells, whereas overexpression of either FADD or caspase-8 induced apoptosis in the absence of FADD (Fig. 4B).

We next investigated the sensitivity of FADD-deficient fibroblasts to various apoptotic stimuli (*16*). As above, WT EF cells became sensitive to TNF in the presence of increasing concentrations of cycloheximide, whereas $FADD^{-/-}$ cells remained resistant to TNF (Fig. 5A). Evidence suggests that oncogenes or chemotherapeutic agents can induce apoptosis by way of the Fas signaling pathway (*17*). We investigated the direct apoptotic effect of c-*myc* by infecting EF cells with a c-*myc*–expressing adenovirus or a control *lacZ*-expressing adenovirus (Fig. 5, B and C) (*18*). However, we observed no significant difference in c-*myc*–induced apoptosis between FADD-expressing and FADD-deficient cells. Similarly, adenovirus E1A protein can induce apoptosis equally well in $FADD^{-/-}$ cells and in WT cells (Fig. 5D) (*18*). Finally, we examined the requirement of FADD for programmed cell death of oncogenically transformed embryonic fibroblasts. Oncogenic transformation by *E1A* and *ras* oncogenes renders mouse EF cells extremely sensitive to the induction of apoptosis by chemotherapeutic drugs (*19*). FADD-deficient cells transformed by *E1A* or *Ras* were as sensitive to various concentrations of adriamycin as their WT counterparts (Fig. 5E) (*20*). These results suggest that FADD is

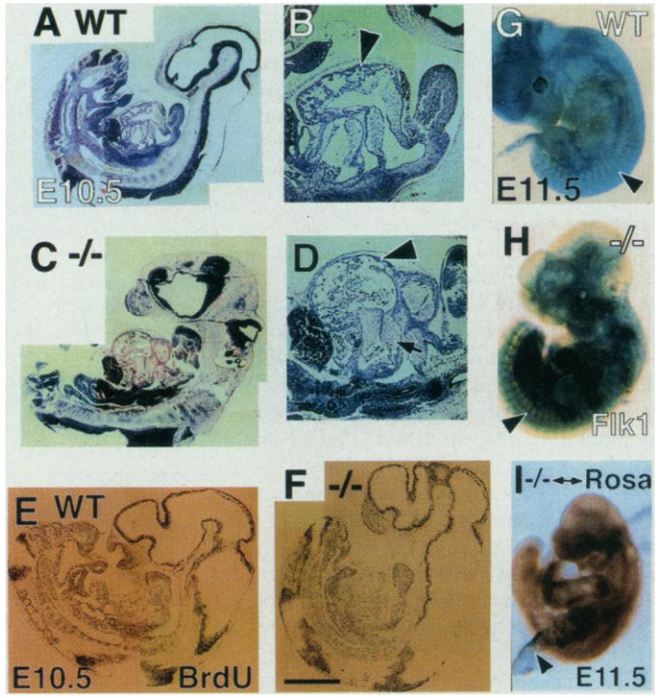

Fig. 3. Histological and chimeric analysis of *FADD* mutant embryos. H&E stainings of longitudinal sections from E10.5 WT (**A** and **B**) and *FADD* mutant embryos (**C** and **D**). (A) Wild-type embryo. General view. (B) Detail showing the ventricular myocardium with its developing trabeculae (arrowhead). General view (C) and detail (D) of a *FADD* mutant embryo, showing the thin ventricular myocardium, the primitive trabeculae (arrowhead), and the normal appearance of the endocardial cushion (arrow). (**E** and **F**) Anti-BrdU staining revealing generalized proliferation in E10.5 WT (E) and *FADD* mutant embryos (F). (**G** and **H**) β-Gal staining showing normal *flk1* expression in the vascular endothelium of E11.5 WT (G, arrowhead) and *FADD* mutant embryos (H, arrowhead). (**I**) β-Gal staining revealing a highly chimeric *FADD*$^{-/-}$*:ROSA 26 lacZ* embryo that reproduces the phenotype observed in $FADD^{-/-}$ embryos obtained from heterozygous breedings. The arrowhead points to WT (blue) cells in the base of the yolk sac. Bar, 500 μm (A, C, and E to I); 200 μm (B and D).

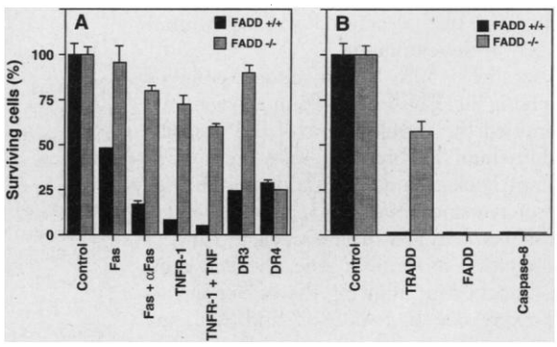

Fig. 4. Defective death signaling in FADD-deficient fibroblasts. (**A**) Wild-type and $FADD^{-/-}$ embryonic fibroblasts were transiently transfected with 2 μg of each death receptor expression vector (TNFR-1, Fas, DR3, or DR4) plus 0.25 μg of pCMV–β-Gal. Fifteen hours after transfection, cells were left untreated or treated with TNF (100 ng/ml) or with an agonistic antibody to Fas (10 μg/ml) for 8 hours. Cells were then fixed and stained with X-Gal. The number of surviving blue cells were counted in 10 randomly selected high-power fields under a microscope and expressed as a percentage relative to the control vector transfection. (**B**) Similar experiments were performed by overexpressing cytoplasmic proteins TRADD, FADD, or caspase-8.

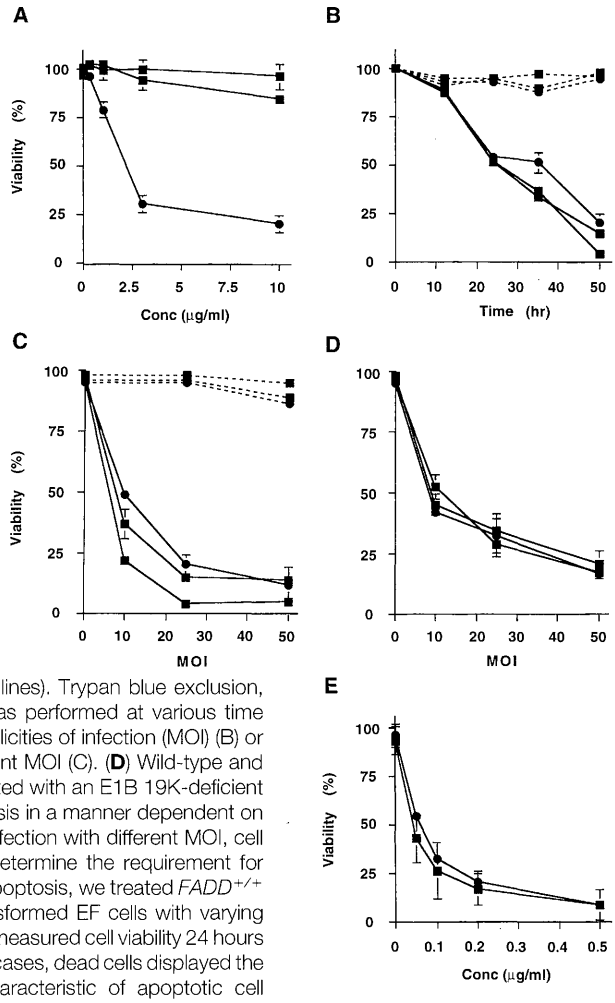

Fig. 5. FADD is required for TNF signaling but is dispensable for both oncogene- and adriamycin-induced apoptosis. For all parts in this figure, $FADD^{+/+}$ was represented by circles and $FADD^{-/-}$ by squares (at least two separate mutant lines are represented). (**A**) $FADD^{+/+}$ and $FADD^{-/-}$ embryonic fibroblasts were left untreated or incubated with recombinant murine TNF (10 ng/ml, Genzyme) plus various concentrations of cycloheximide as indicated. After 24 hours, viable cells were determined by negative stains of trypan blue and 7-amino-actinomycin D (*26*). The latter results were presented as a percentage of untreated controls. (**B** and **C**) Primary $FADD^{+/+}$ or $FADD^{-/-}$ EF cells were infected with adenoviruses expressing either *lacZ* (dotted lines) or c-*myc* (solid lines). Trypan blue exclusion, used to determine cell viability, was performed at various time points after infection with 25 multiplicities of infection (MOI) (B) or 48 hours after infection with different MOI (C). (**D**) Wild-type and FADD-deficient EF cells were infected with an E1B 19K-deficient adenovirus, which induces apoptosis in a manner dependent on E1A (*27*). Forty-eight hours after infection with different MOI, cell viability was determined. (**E**) To determine the requirement for *FADD* in chemotherapy-induced apoptosis, we treated $FADD^{+/+}$ and $FADD^{-/-}$ *E1A*- and *Ras*-transformed EF cells with varying concentrations of adriamycin, and measured cell viability 24 hours later by trypan blue exclusion. In all cases, dead cells displayed the condensed chromatin pattern characteristic of apoptotic cell death (*29*). Data are the means ± SD of four separate $FADD^{-/-}$ EF lines and three separate WT lines.

dispensable for oncogene- or drug-induced apoptosis.

We have shown here that apoptosis-inducing signaling by Fas, TNFR-1, and DR3 (but not by DR4) is impaired in FADD-deficient cells. This supports a report (*15*) that DR4 is a death-domain receptor that kills cells by a FADD-independent mechanism. In our system, FADD was also dispensable for oncogene- or drug-induced apoptosis. Together, these findings are consistent with the hypothesis that, in the absence of FADD, apoptosis induced by oncogenes and chemotherapeutic drugs may utilize DR4, related death receptors, or other pathways. Further investigations are needed to address this issue.

FADD was found to be essential for the viability of the mouse embryo and is specifically required for the development of the ventricular myocardium. The lethality of *FADD* null mutant mice contrasts with the viability of *Fas*- and *TNF-R1*–deficient animals (*21*). It is intriguing that in FADD-deficient embryos the heart is the primary site affected, despite widespread embryonic expression of the gene. This finding is similar to that in mice defective in *N-myc* proto-oncogene (*22*). Another finding that remains to be explained is the developmental retardation of FADD-deficient embryos. Little is known about the embryonic expression pattern of the characterized "death" signaling complexes. It is possible that FADD is engaged in the signaling of an as yet unidentified embryonic death receptor. Alternatively, FADD may transduce signals during embryogenesis from other unknown receptors that function primarily for embryo proliferation and survival. Further investigation of these issues is needed to clarify the roles of FADD during embryogenesis.

REFERENCES AND NOTES

1. S. Nagata, *Cell* **88**, 355 (1997).
2. A. M. Chinnaiyan, K. O'Rourke, M. Tewari, V. M. Dixit, *ibid.* **81**, 505 (1995); M. P. Boldin *et al.*, *J. Biol. Chem.* **270**, 7795 (1995).
3. M. Muzio *et al.*, *Cell* **85**, 817 (1996); M. P. Boldin, T. M. Goncharov, Y. V. Goltsev, D. Wallach, *ibid.*, p. 803.
4. H. Hsu, J. Xiong, D. V. Goeddel, *ibid.* **81**, 495 (1995).
5. H. Hsu, H.-B. Shu, M.-G. Pan, D. V. Goeddel, *ibid.* **84**, 299 (1996).
6. A. M. Chinnaiyan *et al.*, *Science* **274**, 990 (1996); J. Kitson *et al.*, *Nature* **384**, 372 (1996).
7. A targeting vector was designed to replace the entire coding region of *FADD* with the *PGK-neo* resistance expression cassette in reverse orientation to *FADD* transcription. The targeting vector was linearized and electroporated into E14K ES cells. After G418 selection, homologous recombinants were identified by polymerase chain reaction (PCR) and confirmed by Southern (DNA) blot analysis. Chimeric mice were produced by microinjection of *FADD* heterozygous ES cells into E3.5 C57BL6/J blastocysts and transferred to CD1 pseudopregnant foster mothers. Chimeric males were mated with C57BL6/J females (Jackson Laboratories). Germline transmission of the mutant allele was verified by PCR and Southern blot analysis of tail DNA from Agouti coat color F_1 offsprings. PCR, Southern, Northern (RNA), and protein immunoblots were performed according to standard procedures. The mutant phenotype was analyzed in 129/C57BL/6 and 129/CD1 backgrounds; no significant differences were observed.
8. For whole mount in situ hybridization, E8.5 to E10 embryos were fixed and processed according to standard protocols. For radioactive in situ hybridization, E11.5 to E12.5 embryos were isolated and processed as for histological analysis. Hybridization was performed according to standard protocols. The *FADD* probes used were a 1.3-kb full-length murine *FADD* cDNA and a 0.8-kb 3′ untranslated region fragment.
9. Embryos were dissected between E9.5 to E11.5, fixed in 4% paraformaldehyde, dehydrated, embedded in wax, sectioned, and processed for hematoxylin and eosin (H&E) staining according to standard protocols.
10. W.-C. Yeh, J. L. de la Pompa, A. J. Elia, T. W. Mak, unpublished data.
11. To examine the development of the vascular endothelium, a mutation in the *flk1* gene marked with the *lacZ* gene (*23*) was bred to heterozygocity into the FADD mutant background. β-Gal staining was performed according to standard protocols.
12. G. Friedrich and P. Soriano, *Genes Dev.* **5**, 1513 (1991).
13. BrdU (100 μg per gram of body weight) was injected intraperitoneally into pregnant females at E10.5 to E11.5. Females were killed 1 hour after injection, and the embryos were dissected and fixed in 70% ethanol for 2 hours at 4°C, and then processed as for H&E staining. Sections were incubated with a monoclonal antibody to BrdU (Beckton Dickinson) at a 1:10 dilution. Staining was performed as described (*24*), with a biotinylated secondary antibody against mouse immunoglobulin G and avidin-conjugated peroxidase (Vector Laboratory).
14. $FADD^{-/-}$ ES cell lines were generated from G418-resistant $FADD^{+/-}$ ES clones by culturing at an increased G418 concentration (2 mg/ml) (*25*). To assess the developmental potential of the *FADD* mutant ES cells, we injected *ROSA 26 lacZ* (*12*) E3.5 blastocysts with $FADD^{-/-}$ or $FADD^{+/-}$ ES cell clones and transferred them to CD1 pseudopregnant foster mothers. Chimeric embryos were dissected between E10.5 and E11.5 and stained for β-Gal activity.
15. G. H. Pan *et al.*, *Science* **276**, 111 (1997).
16. Primary embryonic fibroblasts were derived from embryos at day 9.5 of gestation and cultured in Dulbecco's modified Eagle's medium supplemented with 5% fetal bovine serum. For treatment with TNF-α and cycloheximide, 3×10^5 cells were plated on each well of a six-well dish a day before treatment. After treatment for 24 hours, cells were trypsinized, all supernatants were collected, and cell viability was determined by trypan blue exclusion and 7-amino-actinomycin D staining (*26*).
17. A.-O. Hueber *et al.*, *Science* **278**, 1305 (1997); C. Friesen, I. Herr, P. H. Krammer, K. M. Debatin, *Nature Med.* **2**, 574 (1996); C. Friesen, S. Fulda, K. M. Debatin, *Leukemia* **11**, 1833 (1997); M. Muller *et al.*, *J. Clin. Invest.* **99**, 403 (1997).
18. For adenovirus experiments, primary mouse embronic fibroblasts (MEFs) were plated at 1×10^5 in 500 μl per 12-well plate, in the presence of varying multiplicities of infection (MOIs) of dl250 (E1B-defective adenovirus)

(27) or a recombinant c-*myc*– or *lacZ*-expressing adenovirus. We constructed c-*myc*–expressing adenovirus by cloning the full-length human c-*myc* cDNA into a replication-deficient Ad5 as described for *lacZ*-expressing adenovirus (28).
19. H. E. Ruley, *Nature* **304**, 602 (1983); S. W. Lowe, H. E. Ruley, T. Jacks, D. E. Housman, *Cell* **74**, 957 (1993); M. E. McCurrach, T. M. Connor, C. M. Knudson, S. J. Korsmeyer, S. W. Lowe, *Proc. Natl. Acad. Sci. U.S.A.* **94**, 2345 (1997).
20. Generation of E1A- and Ras-expressing MEFs was accomplished by mass infection of early-passage MEFs with E1A 13S- and H-rasV12–expressing retroviral vectors as described (19).
21. M. Adachi *et al.*, *Nature Genet.* **11**, 294 (1995); K. Pfeffer *et al.*, *Cell* **73**, 457 (1993).
22. C. Moens, B. R. Stanton, L. F. Parada, J. Rossant, *Development* **119**, 485 (1993).
23. T. P. Yamaguchi, D. J. Dumont, R. A. Conlon, M. L. Breitman, J. Rossant, *Dev. Suppl.* **118**, 489 (1993).
24. Y. Mishina, A. Suzuki, N. Ueno, R. R. Behringer, *Genes Dev.* **9**, 3027 (1995).
25. R. M. Mortensen, D. A. Conner, S. Chao, A. A. Geisterfer-Lowrance, J. G. Seidman, *Mol. Cell. Biol.* **12**, 2391 (1992).
26. I. Schmid, C. H. Uittenbogaart, J. V. Giorgi, *Cytometry* **15**, 12 (1994).
27. E. White and B. Stillman, *J. Virol.* **61**, 426 (1987).
28. W. S. El-Deiry *et al.*, *Cell* **75**, 817 (1993).
29. M. E. McCurrach and S. W. Lowe, unpublished data.
30. We thank V. M. Dixit for DR3 and DR4 vectors and P. H. Krammer for agonistic antibody to Fas; H. Hsu, L.-M. Boucher, and members of T.W.M.'s laboratory for material and instructive discussions; I. del Barco Barrantes and B. Hum for technical assistance; M. Saunders for scientific editing; and I. Ng for administrative support. Supported in part by a grant from the National Cancer Institute of Canada (NCIC) and grant CA13106 from the National Cancer Institute and Medical Research Council of Canada.

14 January 1998; accepted 18 February 1998

Redesigning Enzyme Topology by Directed Evolution

Gavin MacBeath, Peter Kast, Donald Hilvert*

Genetic selection was exploited in combination with structure-based design to transform an intimately entwined, dimeric chorismate mutase into a monomeric, four-helix–bundle protein with near native activity. Successful reengineering depended on choosing a thermostable starting protein, introducing point mutations that preferentially destabilize the wild-type dimer, and using directed evolution to optimize an inserted interhelical turn. Contrary to expectations based on studies of other four-helix–bundle proteins, only a small fraction of possible turn sequences (fewer than 0.05 percent) yielded well-behaved, monomeric, and highly active enzymes. Selection for catalytic function thus provides an efficient yet stringent method for rapidly assessing correctly folded polypeptides and may prove generally useful for protein design.

Several recent studies have focused on reducing the size of protein domains to obtain minimized functional units either by removing secondary structural elements within a domain (*1*) or by converting oligomeric proteins into monomers (*2*, *3*). The latter is particularly challenging when the individual polypeptides are intricately entwined. Monomeric variants of such dimers have been constructed for interleukin-5 by inserting a loop sequence from a homologous protein (*2*) and for λ cro by screening a small subset of carefully designed variants (*3*). A high-resolution crystal structure of the monomeric cro protein, however, revealed significant conformational changes relative to the wild-type dimer (*4*).

The sensitivity of catalytic efficiency to structural perturbations makes minimization of oligomeric enzymes especially difficult. For example, although the active sites of the homodimeric enzyme triosephosphate isomerase do not contain residues from both polypeptides, disruption of the dimer interface results in a >10,000-fold reduction in k_{cat}/K_m (where k_{cat} and K_m are the catalytic rate and Michaelis constants, respectively) (*5*, *6*). Enzymes with active sites at the subunit interface pose even greater challenges. In this context, we considered chorismate mutase (CM), which catalyzes the conversion of chorismate to prephenate in the biosynthesis of L-tyrosine (Tyr) and L-phenylalanine (Phe) with rate accelerations of about 10^6 (*7*). Members of the AroQ class (*8*) of CM are found in a wide variety of bacteria, fungi, and higher plants. Crystallographic studies on a typical AroQ enzyme from *Escherichia coli* (EcCM) have revealed an intriguing homodimeric topology, in which each catalytic domain adopts a four-helix–bundle structure (*9*) (Fig. 1). The long amino-terminal helix (H1) spans the two domains and contributes residues to both active sites of the dimer. We reasoned that if the appropriate loop were inserted in the middle of this helix, a 180° turn could be induced that would allow the amino-terminal half of H1 to fold back and displace the other polypeptide in the dimer to form a monomer (Fig. 1).

The choice of loop sequence is of considerable interest. Previous studies on other four-helix–bundle proteins have shown that there are surprisingly few constraints on the sequence or length of interhelical turns (*10*–*12*). This finding suggests that almost any turn could be used to convert the CM domain into a functional monomer. However, we have recently shown that if residues in an interhelical turn are involved in long-range tertiary interactions, the fraction of acceptable turn sequences can be dramatically reduced (*13*). In the ideal monomer, the inserted loop not only must adopt the appropriate conformation, it also must interact favorably with the newly exposed hydrophobic regions that result from disruption of the subunit interface. Given the exacting conformational control required for efficient enzyme catalysis, prediction of an optimal turn sequence becomes intractable.

By introducing randomized sequences into the AroQ gene and transforming CM-deficient bacteria with the resulting library, acceptable turn sequences that confer high activity should be selectable by genetic complementation (*13*). When this approach was used with EcCM, however, we were unable to obtain stable, monomeric variants (*14*). Although the enzyme active site is preserved in this topological transformation, extensive hydrophobic interactions formed at the subunit interface are lost. This interface comprises much of the core of the folded dimer and hence should contribute significantly to the overall stability of the protein. In support of this notion, denaturation studies show that EcCM undergoes a cooperative transition from folded dimer to unfolded monomer without accumulation of a structured, monomeric intermediate. Analogous results have been obtained with other dimeric proteins in which quaternary structure accounts for most, if not all, of the overall stability (*15*).

We therefore sought a more stable version of the AroQ CM domain. Recent progress in whole genome sequencing has provided access to a plethora of uncharacterized open reading frames (ORFs) from a wide variety of organisms. The complete genomic sequence of the thermophilic archaeon *Methanococcus jannaschii* (*16*) revealed an ORF for a protein with high similarity to EcCM (Fig. 2). No insertions or deletions are apparent, and the active site residues are remarkably conserved. We have subcloned and overexpressed this ORF

The Scripps Research Institute, Departments of Chemistry and Molecular Biology, 10550 North Torrey Pines Road, La Jolla, California, 92037, USA.

*To whom correspondence should be addressed at Department of Chemistry, Swiss Federal Institute of Technology (ETH), CH-8092 Zürich, Switzerland. E-mail: hilvert@org.chem.ethz.ch